Bounds for Linear–Functional Outputs of Coercive Partial Differential Equations : Local Indicators and Adaptive Refinement

J. Peraire [a] and A.T. Patera [b]

[a]Department of Aeronautics and Astronautics, Massachusetts Institute of Technology, Cambridge, MA 02139, USA

[b]Department of Mechanical Engineering, Massachusetts Institute of Technology, Cambridge, MA 02139, USA

We present a framework for the efficient calculation of lower and upper bounds to outputs which are linear functionals of the solutions to symmetric or nonsymmetric second–order coercive partial differential equations. The method is based upon the construction of an augmented Lagrangian, in which the objective is a quadratic energy reformulation of the desired output, and the constraints are the finite element equilibrium conditions and interelement continuity requirements; the bounds are then derived by evoking the dual max-min problem for appropriately chosen candidate Lagrange multipliers. The bound computation comprises two components: several global calculations on a relatively coarse "working" finite–element triangulation $\mathcal{T}_H$ consisting of K_H elements T_H; and $2K_H$ independent T_H–local calculations on a relatively fine "truth" finite–element triangulation $\mathcal{T}_h$.

In this paper we focus on three new developments. First, we introduce a modified energy objective, and hence modified Lagrangian, that permits both more transparent interpretation and more ready generalization. Second, we demonstrate that the bound gap — the difference between the upper and lower bounds for the desired output — can be represented as the sum of positive contributions — local indicators — associated with the elements T_H of $\mathcal{T}_H$. Third, based on these local bound–gap error indicators, we develop adaptive strategies by which to reduce the bound gap — and hence improve our validated prediction for the output of interest — through optimal refinement of $\mathcal{T}_H$. The resulting method is applied to an illustrative problem in linear elasticity.

1. INTRODUCTION

The field of *a posteriori* error estimation and adaptive mesh refinement now has a long history in finite element analysis. The two goals of these related pursuits are, first, inexpensive confirmation of the accuracy of a particular finite element solution, and second, efficient improvement of the finite element solution by optimal adaptive mesh refinement. We now make these notions more precise.

We denote the exact solution to our coercive partial differential equation by u (say, the displacement), and the finite element approximation to u associated with a triangulation $\mathcal{T}_H$ by u_H. The finite element error is thus given by $e \equiv u - u_H$; we denote the (pseudo)metric in which we wish to measure the finite element error by $E(v)$. *A posteriori* procedures provide an estimate, $\mathcal{E}(\mathcal{T}_H)$, for the E–metric of the finite element error, $E(e)$; this estimate $\mathcal{E}(\mathcal{T}_H)$ is typically expressed as the sum of positive contributions $\mathcal{E}_{T_H}$ associated with the K_H elements T_H of the triangulation $\mathcal{T}_H$. The elemental contributions $\mathcal{E}_{T_H}$ are interpreted as local indicators for the purpose of subsequent mesh refinement strategies.

The general approaches to *a posteriori* error estimation may be categorized as "explicit" or "implicit" [3]. Explicit techniques are typically based on residual evaluation and *a priori* approximation and stability results [4,18,7]: the advantage is computational efficiency; the disadvantage is the presence of constants that can not be precisely evaluated. Implicit techniques [11,6,2] are based on the solution of K_H residual–forced T_H–local independent subproblems: the advantage is more precise quantification; the disadvantage is increased complexity and computational effort. Although both explicit and implicit methods typically provide error bounds in the sense that (roughly) there exists a constant $C_{\mathcal{E}}$ independent of $\mathcal{T}_H$ and u such that $E(e) \leq C_{\mathcal{E}}\, \mathcal{E}_{T_H}$ [6,18], the constant $C_{\mathcal{E}}$ is typically not known. In what follows, we shall reserve the term "bound" for estimators for which $C_{\mathcal{E}}$ is known to high accuracy.

Most early work on *a posteriori* error estimation focused, first, on symmetric problems, and second, on the natural energy measure of the error, in which $E(v)$ is chosen to be the norm induced by the symmetric bilinear form associated with the weak formulation of the problem. In this case, very effective explicit and implicit techniques [4,6,18] can be developed that require essentially no regularity assumptions and contain only minimal unknown approximation (and perhaps coercivity) contributions to $C_{\mathcal{E}}$. Furthermore, implicit procedures can be developed [11,2] that provide rigorous *bounds* for the error; the unknown contributions to $C_{\mathcal{E}}$ are reduced to the (typically very small) inaccuracies incurred in the solution of the T_H–local subproblems. Many of these explicit and implicit methods can be readily generalized to nonsymmetric problems [18] and more general error metrics; in contrast, the earlier bound procedures [11,2] are developed only for coercive symmetric problems, and are fundamentally restricted to the natural energy norm.

There has recently been greatly increased interest in the extension of *a posteriori* estimation techniques to error metrics more directly relevant to engineering analysis. In particular, the quantity (or quantities) of interest in engineering studies is not the field variable u, or the error in the energy norm, but rather the output — the system performance metric – that reflects the specific goals and objectives of the design or optimization exercise. To be more precise, we denote this engineering output of interest by s (say, the force over part of the boundary); we further assume that s may be expressed as $s = l^O(u)$, where $l^O(v)$ is a (preferably bounded) affine functional. The finite element approximation to s, s_H, is then given by $s_H = l^O(u_H)$. It is clear that, in order to measure the error in the linear–functional output s, we should choose $E(v) \equiv |l^O(v)|$, since then $E(e) = |l^O(e)| = |l^O(u - u_H)| = |s - s_H|$.

Explicit error estimation techniques — based on the Aubin–Nitsche duality procedure [10] — and associated adaptive refinement strategies are now available for linear–functional outputs, $E(v) \equiv |l^O(v)|$ [7,8,16]. These procedures facilitate the assessment and improvement of finite element predictions for the desired engineering output, s. However, in contrast to explicit indicators for the error in the energy norm, explicit indicators for the error in linear–functional outputs involve, first, more questionable assumptions, and second, more unknown contributions to $C_{\mathcal{E}}$. In particular, $C_{\mathcal{E}}$ now reflects not only undetermined approximation constants, but also regularity hypotheses on the adjoint (dual) variable ψ, *and* potentially inaccurate ($\mathcal{T}_H$) estimates for higher–derivative norms of ψ. Although these explicit techniques for output estimation can certainly yield good results [7,8,16], the goal of confirmation is less well-satisfied. Related reconstruction procedures share similar advantages and disadvantages [5].

We argue that engineering analysis and design is best served by *a posteriori* procedures that eliminate — or at least greatly reduce — the uncertainty in numerical predictions: rigorous and quantitative bounds for $|s - s_H|$ are required if simulation results can be reliably incorporated into the engineering design and optimization process. To this end, we have developed an *implicit* procedure for the prediction of *bounds* for linear–functional outputs of coercive partial differential equations [13,15,14]. The method is based upon the construction of an augmented Lagrangian, in which the objective is a quadratic energy reformulation of the desired output, and the constraints are the finite element equilibrium conditions and interelement continuity requirements; the bounds are then derived by evoking the dual max-min problem for appropriately chosen candidate Lagrange multipliers. As in all implicit procedures, the bound computation comprises two components: several global calculations on the relatively coarse "working" finite–element triangulation $\mathcal{T}_H$; and $2K_H$ independent T_H–local calculations on a relatively fine "truth" finite–element triangulation $\mathcal{T}_h$.

More precisely, our procedure produces quantitative lower and upper bounds, $s_{LO}(\mathcal{T}_H)$ and $s_{UP}(\mathcal{T}_H)$, for $s_h = l^O(u_h)$, the finite element approximation to the output s on the "truth" triangulation $\mathcal{T}_h$. These bounds, in turn, engender a predictor for s_h,

$$s_{pre}(\mathcal{T}_H) = \frac{1}{2}(s_{LO}(\mathcal{T}_H) + s_{UP}(\mathcal{T}_H)), \tag{1}$$

for which

$$|s_h - s_{pre}(\mathcal{T}_H)| \leq \Delta(\mathcal{T}_H). \tag{2}$$

Here

$$\Delta(\mathcal{T}_H) = \frac{1}{2}(s_{UP}(\mathcal{T}_H) - s_{LO}(\mathcal{T}_H)), \tag{3}$$

which we shall denote the (half) *bound gap*. It follows that $|s - s_{pre}|$ (respectively, $|s - s_H|$) is within $|s - s_h|$ of Δ (respectively, of $\Delta + |s_{pre} - s_H|$), and thus $C_{\mathcal{E}}$ is known to within the accuracy of the "truth" mesh. Note that whereas $|s_h - s_H|$ may in fact be smaller than $|s_h - s_{pre}|$, we prefer the predictor s_{pre} since the error *bound* on s_{pre} will be sharper.

Our framework borrows from earlier bound (and other implicit) approaches to *a posteriori* error estimation both in general methodology — the application of quadratic–linear duality theory [11,2] — and in specific technology — the interelement continuity component of the Lagrangian, and relatedly, the construction of equilibrated hybrid fluxes [11,6,2]. However, there are also important differences between the earlier approaches and our new proposal. In particular, earlier bound procedures are based upon a Lagrangian in which the objective function, not the constraints, recovers equilibrium: this reliance on a variational principle limits these approaches to symmetric operators, and, even more fundamentally, to the natural–energy error norm. The Lagrangian in our approach is rather different: the objective is an energy reformulation of the desired output; and the constraints *include* the finite element equilibrium equations, as is common practice in optimization and control applications. These enhancements permit the treatment of much more general error measures, in particular linear–functional outputs, and the consideration of more general equations, in particular nonsymmetric operators [13,15]. Our method has also been extended to the Stokes equations [14,12] and certain nonlinear problems [14], however treatment of general noncoercive or nonlinear systems is not yet possible.

We refer the reader to our earlier publications [13,15,14,12] for a complete description of our approach. In this paper we focus on three important extensions. First, we develop a modified energy objective — and hence modified Lagrangian — that permits both more transparent interpretation (e.g., in terms of Aubin–Nitsche arguments) and more ready generalization (e.g., to inhomogeneous boundary conditions). Second, we demonstrate that the resulting bound gap, $\Delta(\mathcal{T}_H)$ of (3), can be represented as the sum of positive contributions, $\Delta_{T_H}(\mathcal{T}_H)$ — local indicators — associated with the elements of $\mathcal{T}_H$. Third, based on these local bound–gap error indicators, we develop adaptive strategies by which to reduce the bound gap $\Delta(\mathcal{T}_H)$ — and hence the error bound on s_{pre} — through optimal refinement of $\mathcal{T}_H$. We emphasize that our focus is less on error estimation, and more on output prediction: we view the refinement of $\mathcal{T}_H$ primarily as a means by which to improve our bounds. Relatedly, we anticipate that s_{LO} and s_{UP} are the quantities that will be of greatest interest in engineering design; s_{pre} and $\Delta(\mathcal{T}_H)$ are simply convenient artifices through which we can simultaneously sharpen both the lower and upper bounds.

The outline of the remainder of the paper is as follows. In Section 2 we describe the problem that will be the vehicle for our exposition: a general second–order scalar (nonsymmetric) coercive partial differential equation. We also introduce the finite element spaces and bilinear and linear forms that we will require in subsequent sections. In Section 3 we introduce our modified Lagrangian, and describe the associated bound procedure. In Section 4 we identify the local bound–gap indicators, and present our adaptive refinement strategy. Finally, in Section 5, we provide numerical results for a problem in linear elasticity.

2. PROBLEM STATEMENT AND DEFINITIONS

2.1. Governing Equation

We shall consider a scalar second–order linear coercive boundary–value problem characterized by the following variational statement : find $u \in X^D$, and $s \in \mathbb{R}$, such that

$$a(v, u) = l^N(v), \quad \forall v \in X, \tag{4}$$

and

$$s = l^O(u). \tag{5}$$

The field variable u is defined over a domain $\Omega \subset \mathbb{R}^2$ with boundary $\partial\Omega = \Gamma_D \bigcup \Gamma_N$; u must reside in $X^D = \{v + u_D \mid v \in X\}$, where $X = \{v \in H^1(\Omega) \mid v = 0 \text{ on } \Gamma_D\}$.

Here $H^1(\Omega)$ is the usual Sobolev space [1]; Γ_D is the portion of the domain boundary on which the essential (Dirichlet) boundary data, g_D, is imposed; u_D is any function in $H^1(\Omega)$ satisfying the essential boundary conditions, that is, $u_D|_{\Gamma_D} = g_D$; and Γ_N is the portion of $\partial\Omega$ on which natural (normal derivative) boundary conditions are imposed. Also, $a : H^1(\Omega) \times H^1(\Omega) \mapsto I\!R$ is a continuous bi-linear form (not necessarily symmetric), and $l^N : H^1(\Omega) \mapsto I\!R$ (respectively, $l^O : H^1(\Omega) \mapsto I\!R$) is a continuous linear (respectively, affine) functional. (Treatment of unbounded output functionals l^O is considered in [12].)

Finally, we introduce a bilinear symmetric coercive form $a^S : X \times X \mapsto I\!R$, defined as

$$a^S(v,w) = \frac{1}{2}(a(v,w) + a(w,v)), \quad \forall v, w \in X, \tag{6}$$

which induces the energy norm

$$|||v|||^2 = a^S(v,v), \quad \forall v \in X, \tag{7}$$

the "natural" metric in which to measure the finite element error.

2.2. Finite Element Spaces

Two triangulations of the computational domain Ω are considered: the working or design H-mesh, $\mathcal{T}_H$, consisting of K_H elements T_H; and the "truth" h-mesh, $\mathcal{T}_h$, consisting of K_h elements T_h. We require that $\mathcal{T}_h$ is a refinement of $\mathcal{T}_H$; the geometric requirements on $\mathcal{T}_H$ are discussed in the context of our refinement strategy.

To each of these meshes we associate regular piecewise–linear continuous finite element subspaces,

$$X_H = \{v \in X \mid v|_{T_H} \in \mathbf{P}_1(T_H),\ \forall T_H \in \mathcal{T}_H\}, \tag{8}$$

$$X_h = \{v \in X \mid v|_{T_h} \in \mathbf{P}_1(T_h),\ \forall T_h \in \mathcal{T}_h\}, \tag{9}$$

where $\mathbf{P}_1(T)$ denotes the space of linear polynomials over T. Similarly, we define $X_H^D = \{v + u_D \mid v \in X_H\}$, and $X_h^D = \{v + u_D \mid v \in X_h\}$. Note that, by construction, $X_H \subset X_h \subset X$, and $X_H^D \subset X_h^D \subset X^D$.

The algorithms to be presented require that our spaces and forms be expressed as sums of contributions over the H-elements T_H. Towards this end, we introduce the subdomain local spaces $Z_H(T_H)$ and $Z_h(T_H)$,

$$Z_H(T_H) = \mathbf{P}_1(T_H), \quad \forall T_H \in \mathcal{T}_H, \tag{10}$$

$$Z_h(T_H) = \{v|_{T_h} \in \mathbf{P}_1(T_h),\ \forall T_h \in \mathcal{R}_{T_H}\} \cap H^1(T_H), \quad \forall T_H \in \mathcal{T}_H, \tag{11}$$

where $\mathcal{R}_{T_H}$ denotes the set of h-mesh elements contained in T_H. The global representation of $Z_H(T_H)$ and $Z_h(T_H)$ are the "broken" spaces $\hat{X}_H$ and $\hat{X}_h$,

$$\hat{X}_H = \{v \in L_2(\Omega) \mid v|_{T_H} \in Z_H(T_H),\ \forall T_H \in \mathcal{T}_H\}, \tag{12}$$

$$\hat{X}_h = \{v \in L_2(\Omega) \mid v|_{T_H} \in Z_h(T_H),\ \forall T_H \in \mathcal{T}_H\}, \tag{13}$$

where $L_2(\Omega)$ is the space of square-integrable functions.

Finally, the bilinear — $a(\cdot,\cdot)$, $a^S(\cdot,\cdot)$ — and linear — $l^N(\cdot)$, $l^O(\cdot)$ — forms are extended to accept discontinuous functions in the "broken" spaces by redefining these forms as a sum of H-element contributions. For instance, $a(\cdot,\cdot)$ is now written as

$$a(v,w) = \sum_{T_H \in \mathcal{T}_H} a_{T_H}(v|_{T_H}, w|_{T_H}), \quad \forall v, w \in \hat{X}_h; \tag{14}$$

similar expressions are obtained for a^S, l^N, and l^O.

2.3. Continuity Form

Let $\mathcal{E}(\mathcal{T}_H)$ (respectively, $\mathcal{E}(\mathcal{T}_h)$) denote the set of open edges in the triangulation $\mathcal{T}_H$ (respectively, $\mathcal{T}_h$). We can then introduce a space of functions over the element edges $\gamma_H \in \mathcal{E}(\mathcal{T}_H)$,

$$Q_H = \{q|_{\gamma_H} \in \mathbf{P}_1(\gamma_H),\ \forall \gamma_H \in \mathcal{E}(\mathcal{T}_H) \mid q|_{\Gamma_N} = 0\}; \tag{15}$$

analogously,

$$Q_h = \{q|_{\gamma_h} \in \mathbf{P}_1(\gamma_h),\ \forall \gamma_h \in \mathcal{E}(\mathcal{T}_h) \cap \mathcal{E}(\mathcal{T}_H) \mid q|_{\Gamma_N} = 0\}. \tag{16}$$

It follows that $Q_H \subset Q_h \subset H^{-1/2}(\mathcal{E}(\mathcal{T}_H))$; the functions in these spaces can, of course, be discontinuous [9].

Next, we introduce the "jump" bilinear form $b : \hat{X}_h \times Q_h \mapsto I\!R$,

$$b(v,q) = \sum_{\gamma_H \in \mathcal{E}(\mathcal{T}_H)} \int_{\gamma_H} \mathcal{J}_{\gamma_H} v \; q|_{\gamma_H} \; ds, \tag{17}$$

where $\mathcal{J}_{\gamma_H} v$ is the *jump* in v across γ_H when γ_H is an interior edge, and the *trace* of v on γ_H when γ_H is on the boundary $\partial\Omega$. The form $b(\cdot,\cdot)$ can be used to enforce continuity on functions in $\hat{X}_H$ and $\hat{X}_h$; in particular,

$$\begin{aligned} X_H &\equiv \{v \in \hat{X}_H \mid b(v,q) = 0,\ \forall q \in Q_H\}, && (18)\\ X_h &\equiv \{v \in \hat{X}_h \mid b(v,q) = 0,\ \forall q \in Q_h\}. && (19) \end{aligned}$$

Note $b(\cdot,\cdot)$ places no restriction on v on natural boundaries.

3. BOUND PROCEDURE

3.1. $\mathcal{T}_H$ and $\mathcal{T}_h$ Problems

The Galerkin finite element solution on the working mesh, $u_H \in X_H^D$, satisfies

$$a(v, u_H) = l^N(v), \quad \forall v \in X_H; \tag{20}$$

the associated output, s_H, is then computed as

$$s_H = l^O(u_H). \tag{21}$$

Analogously, the Galerkin finite element solution on the "truth" mesh, $u_h \in X_h^D$, satisfies

$$a(v, u_h) = l^N(v), \quad \forall v \in X_h; \tag{22}$$

the associated "truth" output, s_h, is then computed as

$$s_h = l^O(u_h). \tag{23}$$

In the smooth case, $|s - s_H| \sim O(H^2)$, and $|s - s_h| \sim O(h^2)$, where H and h are the diameters of $\mathcal{T}_H$ and $\mathcal{T}_h$, respectively.

It will be assumed that the calculation of u_H, and hence s_H, can be performed at moderate cost. However, the h-mesh will typically be much finer than the H-mesh, in order to ensure that $|s - s_h|$ is suitably small; the computation of u_h and s_h in (22)–(23) will thus, most likely, be impractical. Our objective is, therefore, to devise a procedure that will yield sharp upper and lower bounds for s_h in an affordable manner.

3.2. Lagrangian Formulation

Noting that $u_h - u_H \in X_h$, equation (22) gives

$$a(u_h - u_H, u_h) - l^N(u_h - u_H) = 0, \tag{24}$$

which can be combined with (6) to obtain the following *energy equality*,

$$a^S(u_h - u_H, u_h - u_H) - l^N(u_h - u_H) + a(u_h - u_H, u_H) = 0. \tag{25}$$

Introducing the error $e_h \in X_h$ as the difference between the h-mesh and H-mesh approximations, $e_h = u_h - u_H$, and defining the residual

$$l^E(v) \equiv l^N(v) - a(v, u_H), \quad \forall v \in \hat{X}_h, \tag{26}$$

the energy equality can be rewritten as

$$a^S(e_h, e_h) - l^E(e_h) = 0. \tag{27}$$

Note that $a^S(e_h, e_h)$ is simply $|||e_h|||^2$.

We now introduce the set of functions $\mathcal{S} \subset \hat{X}_h$,

$$\mathcal{S} = \{v \in \hat{X}_h \mid a(w, u_H + v) = l^N(w),\ \forall w \in X_h;\ b(v, q) = 0,\ \forall q \in Q_h\}. \tag{28}$$

We observe that the second constraint enforces continuity and the homogeneous essential conditions, that is, $v \in X_h$, and the first constraint, from (22), then forces $v = e_h$. Therefore, the space $\mathcal{S}$ consists of a single function, e_h. The following trivial minimization statement can then be written,

$$\pm s_h = \min_{v \in \mathcal{S}} \ \kappa(a^S(v, v) - l^E(v)) \pm l^O(u_H + v), \tag{29}$$

where $\kappa \in I\!R_+$ is a non-negative parameter that will be used later to optimize the computed bounds.

The constrained minimization problem (29) suggests the formation of the quadratic-linear Lagrangian $\mathcal{L} : \hat{X}_h \times X_h \times Q_h \mapsto I\!R$,

$$\mathcal{L}^\pm(v, \mu, q) = \ \kappa\ (a^S(v, v) - l^E(v)) \pm l^O(u_H + v) + a(\mu, u_H + v) - l^N(\mu) + b(v, q), \tag{30}$$

which allows us to express $\pm s_h$ as

$$\pm s_h = \inf_{v \in \hat{X}_h} \ \sup_{\mu \in X_h,\ q \in Q_h} \ \mathcal{L}^\pm(v, \mu, q). \tag{31}$$

We know that, at the saddlepoint $(e_h, \psi_h^\pm, p_h^\pm)$,

$$e_h \ = \ \arg \min_{v \in \hat{X}_h} \ [\sup_{\mu \in X_h,\ q \in Q_h} \ \mathcal{L}^\pm(v, \mu, q)], \tag{32}$$

$$(\psi_h^\pm, p_h^\pm) \ = \ \arg \max_{\mu \in X_h,\ q \in Q_h} [\inf_{v \in \hat{X}_h} \mathcal{L}^\pm(v, \mu, q)]. \tag{33}$$

We shall refer to μ as the adjoint (dual) variable, and q as the hybrid flux.

3.3. Duality

From quadratic-linear duality theory [17] and (31) it follows that

$$\pm s_h = \sup_{\mu \in X_h,\ q \in Q_h} \ \inf_{v \in \hat{X}_h} \mathcal{L}^{\pm}(v, \mu, q) \geq \inf_{v \in \hat{X}_h} \mathcal{L}^{\pm}(v, \bar{\mu}_h^{\pm}, \bar{q}_h^{\pm}), \quad \forall \bar{\mu}_h^{\pm} \in X_h,\ \forall \bar{q}_h^{\pm} \in Q_h, \tag{34}$$

with equality for $(\bar{\mu}_h^{\pm}, \bar{p}_h^{\pm}) = (\psi_h^{\pm}, p_h^{\pm})$. Upper and lower bounds for the output s_h, s_{UP} and s_{LO}, respectively, are now readily constructed as

$$s_{LO} \equiv \inf_{v \in \hat{X}_h} \mathcal{L}^{+}(v, \bar{\mu}_h^{+}, \bar{q}_h^{+}) \leq s_h \leq - \inf_{v \in \hat{X}_h} \mathcal{L}^{-}(v, \bar{\mu}_h^{-}, \bar{q}_h^{-}) \equiv s_{UP}. \tag{35}$$

We note that (35) holds for any functions $\bar{\mu}_h^{\pm} \in X_h$ and $\bar{q}_h^{\pm} \in Q_h$. In particular, we will choose these functions to be members of $X_H \subset X_h$ and $Q_H \subset Q_h$.

3.4. Adjoint and Hybrid Flux Calculations

We consider here the problem of determining H-mesh approximations to the adjoint $\psi_h^{\pm}$, $\bar{\mu}_h^{\pm}$, and the hybrid flux $p_h^{\pm}$, $\bar{q}_h^{\pm}$, that will yield sharp bounds. Towards this end, we look for the saddlepoint of the Lagrangian (30) in the subspaces $\hat{X}_H \subset \hat{X}_h$, $X_H \subset X_h$, and $Q_H \subset Q_h$, in particular

$$(\psi_H^{\pm}, p_H^{\pm}) = \arg \max_{\mu \in X_H,\ q \in Q_H} [\inf_{v \in \hat{X}_H} \mathcal{L}^{\pm}(v, \mu, q)], \tag{36}$$

and then set $\bar{\mu}_h^{\pm} = \psi_H^{\pm}$ and $\bar{q}_h^{\pm} = p_H^{\pm}$.

The stationarity conditions for (36) are obtained by requiring that the variations of $\mathcal{L}^{\pm}$ with respect to v, μ, and q vanish: Find $e_H^{\pm} \in \hat{X}_H$, $\psi_H^{\pm} \in X_H$, and $p_H^{\pm} \in Q_H$ such that

$$\begin{aligned} b(w, p_H^{\pm}) &= -\{\kappa\ (2a^S(w, e_H^{\pm}) - l^E(w)) \pm l^O(w) + a(\psi_H^{\pm}, w)\}, \quad \forall w \in \hat{X}_H, &(37)\\ a(w, u_H + e_H^{\pm}) &= l^N(w), \qquad \forall w \in X_H, &(38)\\ b(e_H^{\pm}, q) &= 0, \qquad \forall q \in Q_H. &(39) \end{aligned}$$

First, equation (39) forces $e_H^{\pm} \in X_H$, which combined with (38) and (20) implies that $e_H^{\pm} = 0$. Next, equation (37) must be satisfied for all $w \in \hat{X}_H$, and thus, for all $w \in X_H \subset \hat{X}_H$. The adjoint, $\psi_H^{\pm} \in X_H$, can therefore be determined (precisely as in Aubin–Nitsche procedures [7]) as

$$a(\psi_H, w) = -l^O(w), \quad \forall w \in X_H, \tag{40}$$

with $\psi_H^{\pm} = \pm \psi_H$. Note that, in deriving (40), we exploit, first, $l^E(w) = 0$, $\forall w \in X_H$, which follows from (20), and second $b(w, p_H^{\pm}) = 0$, $\forall w \in X_H$, from (18).

Finally, equation (37) can now be evoked to determine the hybrid fluxes $p_H^{\pm} \in Q_H$,

$$b(w, p_H^{\pm}) = \kappa l^E(w) \mp l^O(w) - a(\psi_H^{\pm}, w), \quad \forall w \in \hat{X}_H. \tag{41}$$

Alternatively, we can find $p_{0H} \in Q_H$ and $p_{1H} \in Q_H$ such that

$$\begin{aligned} b(w, p_{0H}) &= -l^O(w) - a(\psi_H, w), \quad \forall w \in \hat{X}_H, &(42)\\ b(w, p_{1H}) &= l^E(w)\ (= l^N(w) - a(w, u_H)), \quad \forall w \in \hat{X}_H, &(43) \end{aligned}$$

and then set $p_H^{\pm} = \pm p_{0H} + \kappa p_{1H}$.

Note that p_{0H} *equilibrates* the H-mesh adjoint (40), whereas p_{1H} *equilibrates* the original H-mesh solution (20).

Equations (42) and (43) represent a solvable but indeterminate system. The computation of an acceptable compatible solution is known as the *equilibration problem*. We follow here the approach proposed in [11,6,2], which involves the solution of an indeterminate system at each vertex of the $\mathcal{T}_H$ grid, the size of which is given by the number of edges that meet at the vertex. Details about this procedure can be found elsewhere [15,12].

3.5. Local Problems

We consider here the solution of the minimization problems in (35). The minimizers of $\mathcal{L}^{\pm}(v, \psi_H^{\pm}, p_H^{\pm})$, $\hat{e}_h^{\pm} \in \hat{X}_h$, will satisfy the following stationarity condition,

$$2\kappa a^S(w, \hat{e}_h^{\pm}) = \kappa l^E(w) \mp l^O(w) - a(\psi_H^{\pm}, w) - b(w, p_H^{\pm}), \quad \forall w \in \hat{X}_h, \tag{44}$$

which we recognize as $2K_H$ independent T_H–local symmetric Neumann (or Robin) subdomain problems. Note that, although a^S is coercive over $X_h \times X_h$, it is typically only semi-definite over $\hat{X}_h \times \hat{X}_h$; however, thanks to (41), if the singular modes of $\hat{X}_h$ are shared by $\hat{X}_H$, (44) will be solvable, and our bounds finite. The equations for $\hat{e}_h^{+}$ and $\hat{e}_h^{-}$ can be rearranged into the following problems for $\hat{e}_{0h}$ and $\hat{e}_{1h}$,

$$\begin{aligned} 2a^S(w, \hat{e}_{0h}) &= -l^O(w) - a(\psi_H, w) - b(w, p_{0H}), \qquad \forall w \in \hat{X}_h, & (45)\\ 2a^S(w, \hat{e}_{1h}) &= l^N(w) - a(w, u_H) - b(w, p_{1H}), \qquad \forall w \in \hat{X}_h, & (46) \end{aligned}$$

from which we construct $\hat{e}_h^{\pm} = \pm\frac{1}{\kappa}\hat{e}_{0h} + \hat{e}_{1h}$. Note that $\hat{e}_{0h}$ and $\hat{e}_{1h}$ are related to the error in the adjoint ψ_H, and the error in the solution u_H, respectively.

3.6. Bounds Calculation

To evaluate the bounds, it remains only to insert the computed values for $\hat{e}_h^{\pm}$, $\psi_H^{\pm}$, and $p_H^{\pm}$ into our Lagrangian. In particular, evoking (44) with $w = \hat{e}_h^{\pm}$, and (20) with $w = \psi_H^{\pm}$, we obtain from (35)

$$\begin{aligned} s_{UP}(\mathcal{T}_H, \kappa) &\equiv -\mathcal{L}^{-}(\hat{e}_h^{-}, \psi_H^{-}, p_H^{-}) = l^O(u_H) + \kappa a^S(\hat{e}_h^{-}, \hat{e}_h^{-}), & (47)\\ s_{LO}(\mathcal{T}_H, \kappa) &\equiv \mathcal{L}^{+}(\hat{e}_h^{+}, \psi_H^{+}, p_H^{+}) = l^O(u_H) - \kappa a^S(\hat{e}_h^{+}, \hat{e}_h^{+}), & (48) \end{aligned}$$

where the arguments of s_{UP} and s_{LO} indicate that the quality of the bounds depends on the working mesh $\mathcal{T}_H$ and the parameter κ. Note that (47), (48) indicate that our bounds for s_h are also bounds for s_H. Note also that, for the "compliance" case — $a(\cdot,\cdot)$ symmetric, $l^O = l^N$, homogeneous essential conditions, and $\kappa = 1$ — $\psi^+ = -u_H$ and $p_H^+ = 0$; it follows that $\hat{e}_h^+ = 0$, and thus $s_{LO} = l^O(u_H)$.

We can also express our bounds in terms of $\hat{e}_{0h}$, $\hat{e}_{1h}$,

$$\begin{aligned} s_{UP}(\mathcal{T}_H, \kappa) &= l^O(u_H) - 2a^S(\hat{e}_{0h}, \hat{e}_{1h}) + \frac{1}{\kappa}a^S(\hat{e}_{0h}, \hat{e}_{0h}) + \kappa a^S(\hat{e}_{1h}, \hat{e}_{1h}), & (49)\\ s_{LO}(\mathcal{T}_H, \kappa) &= l^O(u_H) - 2a^S(\hat{e}_{0h}, \hat{e}_{1h}) - \frac{1}{\kappa}a^S(\hat{e}_{0h}, \hat{e}_{0h}) - \kappa a^S(\hat{e}_{1h}, \hat{e}_{1h}), & (50) \end{aligned}$$

which we recall is valid for any positive value of the parameter κ. The choice of κ will affect the (half) bound gap,

$$\Delta(\mathcal{T}_H, \kappa) \equiv \frac{1}{2}(s_{UP} - s_{LO}) = \frac{1}{\kappa}a^S(\hat{e}_{0h}, \hat{e}_{0h}) + \kappa a^S(\hat{e}_{1h}, \hat{e}_{1h}), \tag{51}$$

but will not affect the output predictor,

$$s_{pre}(\mathcal{T}_H) \equiv \frac{1}{2}(s_{UP} + s_{LO}) = l^O(u_H) - 2a^S(\hat{e}_{0h}, \hat{e}_{1h}). \tag{52}$$

(Recall from (2) that $|s_h - s_{pre}(\mathcal{T}_H)| \leq \Delta(\mathcal{T}_H)$.) Since $\hat{e}_{0h}$ and $\hat{e}_{1h}$ do not depend on the choice of κ, we can readily find that κ which minimizes the bound gap, and hence renders the lower and upper bounds as sharp as possible. This procedure gives

$$\kappa^* = \sqrt{\frac{a^S(\hat{e}_{0h}, \hat{e}_{0h})}{a^S(\hat{e}_{1h}, \hat{e}_{1h})}}, \tag{53}$$

and the optimized bounds

$$\begin{aligned} s_{UP}(\mathcal{T}_H, \kappa^*) \equiv s_{UP}(\mathcal{T}_H) &= l^O(u_H) - 2a^S(\hat{e}_{0h}, \hat{e}_{1h}) + 2\, |||\hat{e}_{0h}|||\ |||\hat{e}_{1h}|||, & (54)\\ s_{LO}(\mathcal{T}_H, \kappa^*) \equiv s_{LO}(\mathcal{T}_H) &= l^O(u_H) - 2a^S(\hat{e}_{0h}, \hat{e}_{1h}) - 2\, |||\hat{e}_{0h}|||\ |||\hat{e}_{1h}|||, & (55) \end{aligned}$$

and associated bound gap

$$\Delta(\mathcal{T}_H, \kappa^*) \equiv \Delta(\mathcal{T}_H) = 2\, |||\hat{e}_{0h}|||\ |||\hat{e}_{1h}|||. \tag{56}$$

(Note that, in the compliance case, $\kappa^* = 1$.) We thus see that our procedure is a *bound formulation* of the classical Aubin–Nitsche result; an implicit counterpart to existing explicit schemes for linear functional outputs [7,8]. In the smooth case we expect that $|||\hat{e}_{0h}|||$ and $|||\hat{e}_{1h}|||$ will each be $O(H)$, and thus $\Delta(\mathcal{T}_H) \sim O(H^2)$ will vanish at the same rate as $|s - s_H|$ as $H \to 0$.

For the special situation in which $\kappa = 1$ and $l^O(u_H + v) \equiv l^E(v)$, we see from (27) that our upper bound corresponds to an upper bound for the error in the energy norm, and thus in this case our method is a (rather trivial) extension of the method of [2] to nonsymmetric operators. (The lower bound is zero, consistent with our compliance result.) Note that, for both the symmetric and nonsymmetric problems, $\psi_H^- = 0$, however only for the symmetric problem is $\psi_h^- = 0$. It follows that only for the symmetric problem is e_h the minimizer of $\mathcal{L}^\pm(v, \psi_H^- {=} 0, \,\cdot\,)$ ($= 2J(v)$ of [2] *in this particular case*) over all $v \in X_h$. This highlights the distinction between our *energy functional* [14], $a^S(v,v) - l^E(v) \pm l^O(u_H + v)$, and a variational principle: the former is only required to *evaluate* to $l^O(u_h)$ for $v = e_h$, while the latter must attain its *minimum* $l^O(u_h)$ at $v = e_h$. We are able to consider more general objective functions since the task of enforcing $v = e_h$ has been moved to a constraint.

Finally, we briefly summarize computational complexity. On $\mathcal{T}_H$, we require two global calculations, one for u_H and one for ψ_H, and two (local) hybrid flux equilibrations. On $\mathcal{T}_h$ we need only invert $2K_H$ independent T_H-local *symmetric* Neumann operators. It follows from the superlinearity of most general solution algorithms that the effort to compute our bounds will be much less than the effort to directly compute u_h and s_h. Note that for each additional output of interest, we require only *one* additional global calculation on $\mathcal{T}_H$, and *one* additional equilibration, and only $1K_H$ additional T_H-local Neumann problems.

4. ADAPTIVITY

4.1. Local Indicators

The procedure presented to calculate bounds can be implemented on any pair of meshes, $\mathcal{T}_H$ and $\mathcal{T}_h$, which satisfy the requirement that $\mathcal{T}_h$ is a refinement of $\mathcal{T}_H$. Since the cost of computing the bounds is essentially a function of the number of elements K_H in $\mathcal{T}_H$, it is desirable to construct *optimized* triangulations that maximize the bound accuracy (minimize the bound gap) for a given number of degrees-of-freedom. In this section we present an algorithm for generating such optimized grids in an adaptive iterative manner.

We first note that the bound gap (56) can be expressed as a sum of elemental contributions,

$$\Delta(\mathcal{T}_H) = \sum_{T_H \in \mathcal{T}_H} \Delta_{T_H}(\mathcal{T}_H), \tag{57}$$

where

$$\Delta_{T_H}(\mathcal{T}_H) = \frac{1}{\kappa^*} a^S_{T_H}(\hat{e}_{0h}, \hat{e}_{0h}) + \kappa^* a^S_{T_H}(\hat{e}_{1h}, \hat{e}_{1h}) \tag{58}$$

$$= \sqrt{\frac{a^S(\hat{e}_{1h}, \hat{e}_{1h})}{a^S(\hat{e}_{0h}, \hat{e}_{0h})}}\, a^S_{T_H}(\hat{e}_{0h}, \hat{e}_{0h}) + \sqrt{\frac{a^S(\hat{e}_{0h}, \hat{e}_{0h})}{a^S(\hat{e}_{1h}, \hat{e}_{1h})}}\, a^S_{T_H}(\hat{e}_{1h}, \hat{e}_{1h}) \tag{59}$$

Note that $\Delta_{T_H}(\mathcal{T}_H)$ is non-negative and can thus be directly interpreted as the *contribution* to the bound gap from element T_H.

We can now describe our iterative adaptive strategy. Starting from an initial grid $\mathcal{T}_H^0$ with bound gap $\Delta(\mathcal{T}_H^0)$, we generate a sequence of triangulations $\{\mathcal{T}_H^k,\ k = 1, 2, \ldots\}$, with corresponding bound gaps $\{\Delta(\mathcal{T}_H^k),\ k = 1, 2, \ldots\}$, such that each triangulation $\mathcal{T}_H^k$ is a refinement of the preceding triangulation $\mathcal{T}_H^{k-1}$. The approach does not guarantee that $\Delta(\mathcal{T}_H^k) \leq \Delta(\mathcal{T}_H^{k-1})$ for any particular k, but it does ensure that, for a sufficiently large k, $\Delta(\mathcal{T}_H^k) \leq \Delta^{targ}$, where $\Delta^{targ} > 0$ is a specified positive gap target.

In order to identify the elements in $\mathcal{T}_H^{k-1}$ that need to be refined, we first calculate the largest elemental contribution Δ_{max}^{k-1} to the bound gap $\Delta(\mathcal{T}_H^{k-1})$,

$$\Delta_{max}^{k-1} = \max_{T_H \in \mathcal{T}_H^{k-1}} \Delta_{T_H}(\mathcal{T}_H^{k-1}), \tag{60}$$

and then select for refinement all those elements $T_H \in \mathcal{T}_H^{k-1}$ for which

$$\Delta_{T_H}(\mathcal{T}_H^{k-1}) \geq \alpha \Delta_{max}^{k-1}. \tag{61}$$

Here, $0 < \alpha < 1$ is a parameter which controls the fraction of elements to be refined at each iteration. At present, this parameter is specified *a priori*, and is independent of k. More sophisticated strategies for choosing α can, of course, be devised; for instance, we can determine α^k such that, based on *a priori* scalings, a given target gap $\Delta^{targ,k}$ should be satisfied by the refined grid $\mathcal{T}_H^k$.

The refinement process is terminated when a selected accuracy goal is achieved. In the applications that follow, the accuracy measure is the relative (half) bound gap θ^k,

$$\theta^k = \frac{\Delta(\mathcal{T}_H^k)}{s_{pre}(\mathcal{T}_H^k)}. \tag{62}$$

The iteration is thus halted when $\theta^k \leq \theta^{obj}$ where θ^{obj}, is the prescribed accuracy.

4.2. Grid Refinement

The triangulation $\mathcal{T}_H^k$ is generated from $\mathcal{T}_H^{k-1}$ by refinement of the selected triangles (T_H such that $\Delta_{T_H}(\mathcal{T}_H^{k-1}) > \alpha\Delta_{max}^{k-1}$) triangles into *four* similar triangles. This refinement strategy leads to the generation of *hanging nodes* whenever only one of the two triangles sharing an edge is refined. Since an element T_H with a hanging node — a node on ∂T_H which is *not* a vertex of T_H — requires special computational treatment, we permit only one hanging node per element. We thus, first, refine all those elements satisfying equation (61), and then, in addition, recursively refine those elements that have more than one hanging node. At the conclusion of the process, only two types of elements (having either zero or one hanging node) are present. This approach has the benefit that fairly smooth grids are generated, and that only one type of *special* element needs to be developed.

We note that in unrefined elements the T_H-local operators required in (45), (46) are unchanged from iteration $k-1$ to iteration k. This can be used (in conjunction with direct solution methods) to greatly reduce the cost of subsequent refinements.

4.3. Computational Treatment of Hanging Nodes

Consider a triangle with nodes IJK, with a hanging node M located at the midpoint of edge IJ. It follows from (8) that functions in the finite element space X_H^k associated with the triangulation $\mathcal{T}_H^k$ must be continuous. This implies that any function v in X_H^k must vary linearly over the edge IJ, and thus the value of v at M, v_M, will be determined by the values of v at nodes I and J, v_I and v_J, respectively: $v_M = (v_I + v_J)/2$.

A convenient way to treat hanging nodes when solving equations (20) and (40) is to split the triangle IJK into two standard triangles, IMK and MJK, and to proceed in forming the equation system as if M is a standard node. The equation corresponding to the hanging node M can then be conveniently removed from the system by simple row and column operations: one half of row (respectively, column) M is added to rows (respectively, columns) I and J. Performing this operation for every hanging node produces a system that involves only the true unknowns at the standard nodes. Once the system has been solved, the value of the solution at the hanging nodes is easily recovered.

The next step is the solution of the equilibration problems (42) and (43). Here, we also follow the approach of splitting the triangle IJK into the two triangles, IMK and MJK. The equilibration problem, however, can not be carried out in the usual fashion, since the solution at points I, M, and J will generally not be in equilibrium. In fact, it can be shown that the effect of constraining v_M to be the average of v_I and v_J is equivalent to the application of a "force" $\lambda \in I\!R$ at nodes I and J, and a force -2λ at node M. The magnitude of λ — a Lagrange multiplier — can be determined from the load imbalance at node M after all elements sharing M have been considered. With the addition of the elemental forces to element IMK (respectively, MJK) — λ to node I (respectively, J) and $-\lambda$ to node M — the flux equilibration procedure (42) and (43) can then be carried out in its standard form.

Finally, the two elements IMK and MJK are combined into the original element IJK before the local Neumann problems (45) and (46) are solved. The element hybrid fluxes over the edge MK will cancel, and the equilibrating forces λ introduced to compute the hybrid fluxes can be removed; the equations (45) and (46) remain solvable, since the sum and moment of the λ forces applied is zero. The only special treatment in this case is that the hybrid flux over the edge IJ is defined in terms of two piecewise linear functions.

5. RESULTS

Results are presented for the two-dimensional generalized planar stress linear elasticity equations. Although here the solution field u is the displacement vector, the theory presented for the scalar problem can be trivially extended to handle this case [15]. The particular problem considered is that of one-fourth of a symmetrically loaded plate with two rectangular holes, as shown in Figure 1. The domain boundaries are denoted by $\Gamma^j,\ j = 1, \ldots, 6$. A horizontal unit distributed force is applied along Γ^3, and homogeneous essential boundary conditions are enforced on the normal displacement on Γ^1, Γ^2, and Γ^5; stress-free condition apply on all other boundaries and components. The Young's modulus and Poisson ratio are taken to be 1 and 0.3, respectively.

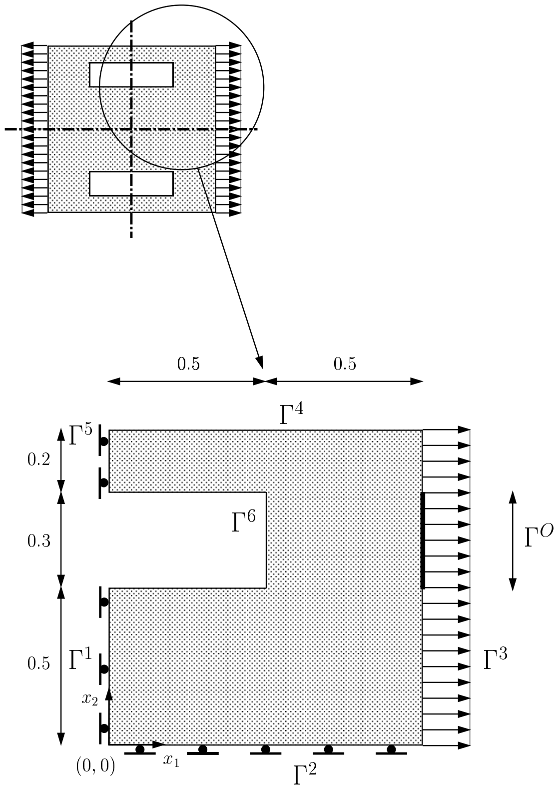

Figure 1. Geometry for linear elasticity example: one–fourth of a symmetrically loaded plate with two square holes. A normal traction is applied on Γ^3; the outputs of interest are the normal force on Γ^5, and the average normal displacement over the segment $\Gamma^O \subset \Gamma^3$.

Two outputs are considered: the normal force on the boundary segment Γ^5, denoted by s^1, and the average horizontal displacement over the segment Γ^O, denoted by s^2. we express the force output as a bounded linear functional [15],

$$l_1^O(v) = \int_\Omega \frac{\partial \chi_i}{\partial x_j} \sigma_{ij}(u) dA, \tag{63}$$

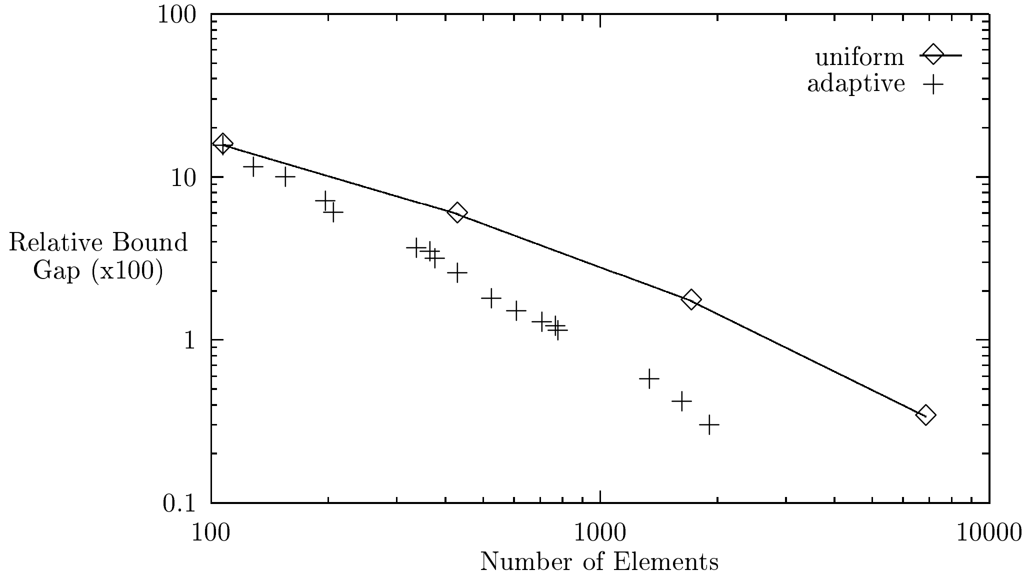

Figure 2. Bound gap $\Delta(\mathcal{T}_H)$ as a function of the number of elements K_H, for the force output s^1, for meshes generated using uniform and adaptive refinement.

where summation over repeated indices is assumed $(i, j = 1, 2)$, $\sigma_{ij}(u)$ is the stress tensor, and χ_i is a vector function defined as

$$\chi_1 = \begin{cases} 1 - 2x_1 & : \quad (x_1, x_2) \in \Omega' \\ 0 & : \quad (x_1, x_2) \in \Omega/\Omega' \end{cases}, \qquad \chi_2 = 0. \tag{64}$$

Here $\Omega' = \{(x_1, x_2)|\ 0 \leq x_1 \leq 0.5, 0.8 \leq x_2 \leq 1.0\}$. Since there are no volume forces, or tractions applied at either Γ^4 or Γ^6, (63) is equivalent, for sufficiently smooth functions, to the integral along Γ^5 of the horizontal component of the traction vector. The average normal displacement linear functional is simply written as

$$l_2^O(v) = \frac{1}{|\Gamma^O|} \int_{\Gamma^O} v_1 ds, \tag{65}$$

which is bounded for all Γ^O of non-zero measure.

The same initial triangulation $\mathcal{T}_H^0$ and "truth" mesh $\mathcal{T}_h$ have been considered for both outputs. The initial triangulation consists of 108 triangles. The "truth" mesh has been generated from this initial triangulation by four refinement interactions in which *all* triangles are subdivided; thus, the number of elements in the "truth" mesh is $27,648 = 108 \times 4^4$. In the adaptive process, elements were selected for refinement based on equation (61) with $\alpha = 0.3$ for all the iterations. The accuracy goal, θ^{obj}, for the relative (half) bound gap, (62), is 0.003 (or 0.3%).

For the force output s^1, 16 refinement iterations are required starting from a relative bound gap of 15.64%; only 12 refinement iterations are required for the displacement

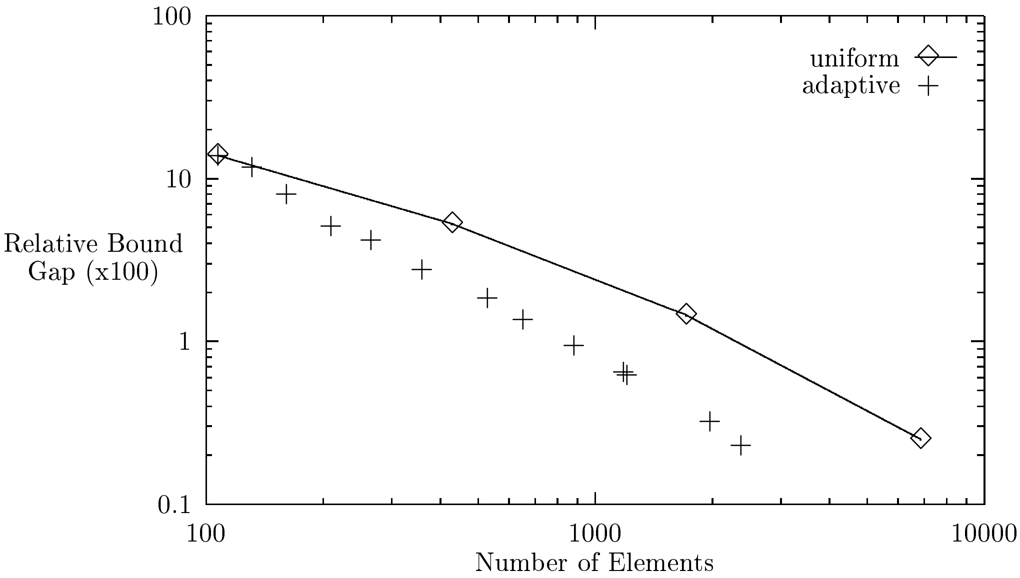

Figure 3. Bound gap $\Delta(\mathcal{T}_H)$ as a function of the number of elements K_H, for the displacement output s^2, for meshes generated using uniform and adaptive refinement.

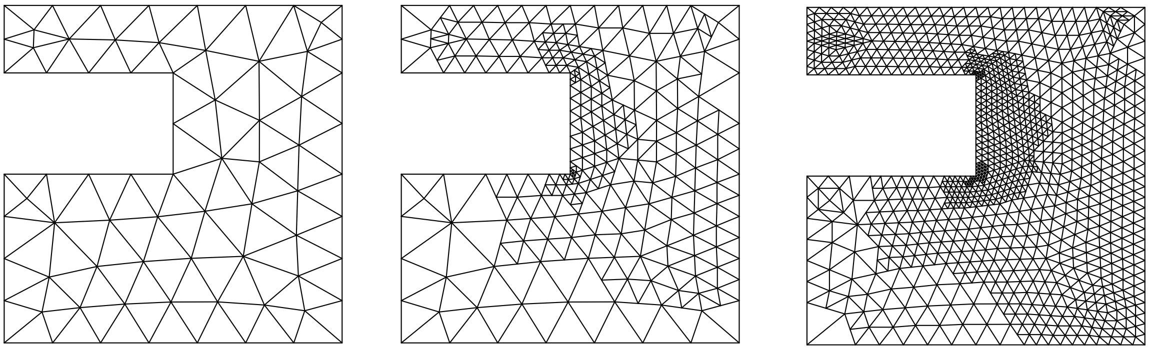

Figure 4. Adaptively generated meshes for normal force output s^1. Figure shows $\mathcal{T}_H^0$, $\mathcal{T}_H^8$, and $\mathcal{T}_H^{16}$, with $K_H^0 = 108$, $K_H^8 = 432$, and $K_H^{16} = 1917$ elements; predicted outputs are $s_{pre}^{1,0} = -0.3198$, $s_{pre}^{1,8} = -0.3215$, and $s_{pre}^{1,16} = -0.3220$; and relative bound gaps are $\theta^{1,0} = 15.64\%$, $\theta^{1,8} = 2.59\%$, and $\theta^{1,16} = 0.30\%$.

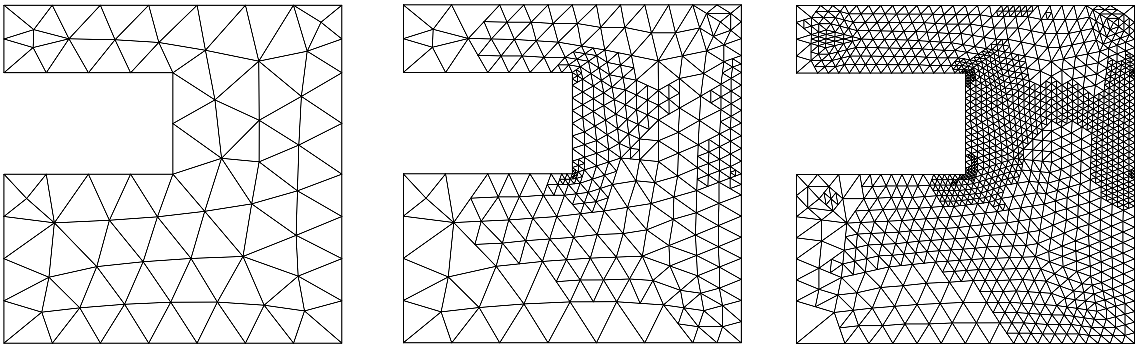

Figure 5. Adaptively generated meshes for the displacement output s^2. Figure shows $\mathcal{T}_H^0$, $\mathcal{T}_H^6$, and $\mathcal{T}_H^{12}$, with $K_H^0 = 108$, $K_H^6 = 531$, and $K_H^{12} = 2382$ elements; predicted outputs are $s_{pre}^{2,0} = 0.4056$, $s_{pre}^{2,6} = 0.4204$, and $s_{pre}^{2,12} = 0.4226$; and relative bound gaps are $\theta^{2,0} = 13.82\%$, $\theta^{2,6} = 1.83\%$, and $\theta^{2,12} = 0.23\%$.

output s^2, for which the initial relative bound gap is 13.82%. Figures 2 and 3 show the relative bound gap as a function of the number of elements, at each adaptive iteration, for the force and displacement outputs, respectively. We also show the bound gap computed for a sequence of grids obtained by uniform refinement, the finest of which still has four times fewer elements than the "truth" mesh $\mathcal{T}_h$. For both outputs we observe that, the uniformly refined meshes require approximately four times as many elements as the adaptive meshes for comparable levels of accuracy.

We note that, say for the force output, $|(s_{pre}^{1,16} - s_h)/s_{pre}^{1,16}| = 0.0001$, whereas $\theta^{1,16} = 0.003$, and thus the effectivity of the estimator in the classical sense is not as good as we may hope, even though the convergence *rate* of $\Delta(\mathcal{T}_H)$ is optimal. We emphasize, however, that our bounds provide *certainty* that $|(s_{pre}^{1,16} - s_h)/s_{pre}^{1,16}| \leq 0.003$ — and more importantly, that s_h lies between $s_{LO}^{1,16} = -0.3230$ and $s_{UP}^{1,16} = -0.3211$ — without calculating s_h on the uniformly highly refined (and hence expensive) "truth" mesh $\mathcal{T}_h$. Future work will address techniques by which to reduce the ratio $\Delta(\mathcal{T}_H)/|s_h - s_{pre}|$ as $H \to 0$; this, in turn, will permit to achieve θ^{obj} on coarser meshes $\mathcal{T}_H$.

Finally, in Figures 4 and 5, we show the initial, an intermediate, and the final adaptive triangulations obtained for the force and displacement outputs, respectively. Refinement around the singular re-entrant corners is apparent in both cases but, in addition, in the displacement output case, further refinement is observed near the points where l_2^O is "discontinuous".

In conclusion, we have shown that the goals of *validated outputs* and *optimal mesh refinement* can be simultaneously satisfied within our bounds framework. Clearly much work is required to translate these "end results" into computationally effective algorithms; our focus in the current paper is on the development of the appropriate foundation.

6. ACKNOWLEDGEMENTS

Support for this work has been provided by DARPA and ONR under Grant N00014-91-J-1889, the AFOSR under Grant F49620-97-1-0052, and NASA under Grants NAG 1-1613, NAG 4-105, NAG 1-1587, and NCC 3-483.

REFERENCES

1. R.A. Adams, *Sobolev Spaces*, Academic Press, New York, 1975.
2. M. Ainsworth and J.T. Oden, *A unified approach to* a posteriori *error estimation using element residual methods*, Numer. Math., **65** (1993), pp. 23-50.
3. M. Ainsworth and J.T. Oden, A posteriori *error estimation in finite element analysis*, TICAM Report 96-19, 1996.
4. I. Babuška and W.C. Rheinboldt, *Analysis of optimal finite element meshes in* $\mathbb{R}^1$, Math. Comp., **33** (1979), pp. 435–463.
5. I. Babuška, T. Strouboulis, C.S. Upadhyay, and S.K. Gangaraj, A posteriori *estimation and adaptive control of the pollution error in the h–version of the finite element method*, Int. J. Numer. Methods Engrg., **38** (1995), pp. 4207–4235.
6. R.E. Bank and A. Weiser, *Some* a posteriori *error estimators for elliptic partial differential equations*, Math. Comp., **44**:170 (1985), pp. 283–301.
7. R. Becker and R. Rannacher, *Weighted* a posteriori *error control in finite element methods*, IWR Preprint 96–1 (SFB 359), Heidelberg, 1996.
8. R. Becker and R. Rannacher, *A feedback approach to error control in finite element methods: basic analysis and examples*, IWR Preprint 96–52 (SFB 359), Heidelberg, 1996.
9. F. Brezzi and M. Fortin, *Mixed and Hybrid Finite Element Methods*, Springer–Verlag, New York, 1991.
10. K. Eriksson and C. Johnson, *An adaptive finite element method for linear elliptic problems*, Math. Comp., **50** (1988), pp. 361-383.
11. P. Ladeveze and D. Leguillon, *Error estimation procedures in the finite element method and applications*, SIAM J. Numer. Anal., **20** (1983), pp. 485–509.
12. M. Paraschivoiu, A Posteriori *Finite Element Bounds for Linear–Functional Outputs of Coercive Partial Dfferential Equations and of the Stokes Problem*, Ph.D. Thesis, Department of Mechanical Engineering, M.I.T., October, 1997.
13. M. Paraschivoiu and A.T. Patera, *A hierarchical duality approach to bounds for the outputs of partial differential equations,* Comp. Meth. Appl. Mech. Engrg., to appear.
14. M. Paraschivoiu, J. Peraire, Y. Maday, and A.T. Patera, Fast bounds for Outputs of Partial Differential Equations, in Proceedings Workshop on Optimal Design and Control, Washington, D.C., ed. J. A. Burns, E. M. Cliff, and B. Grossman, to appear.
15. M. Paraschivoiu, J. Peraire, and A.T. Patera, A posteriori *finite element bounds for linear–functional outputs of elliptic partial differential equations*, Comp. Meth. Appl. Mech. Engrg., to appear.
16. R. Rannacher and F.-T. Suttmeier, *A feedback approach to error control in finite element methods: application to linear elasticity*, Preprint 96–42 (SFB 359), Heidelberg, 1996.

17. G. Strang, *Introduction to Applied Mathematics*, Wellesley–Cambridge Press, Wellesley, Massachusetts, 1986.
18. R. Verfürth, A posteriori *error estimation and adaptive mesh–refinement techniques*, J. Comp. Appl. Math., **50** (1994), pp. 67–83.